

Lecture 5 - Photodetectors and Noise

Many different types of detector can be used to measure the amount of electromagnetic radiation that falls upon them. In this lecture I shall begin by giving a general introduction to the various popular detectors, pointing out their specific applications. I shall then look in more detail at three classes of detector which are of major importance in communication systems, photomultiplier tubes, semiconducting devices such as pn-junctions and p-i-n diodes, and avalanche photodiodes. I shall also discuss the technology behind CCD detectors.

1 Thermal Detectors

In thermal detectors, radiation is absorbed in the active element, and this changes the temperature of the device. The change in temperature then gives rise to a change in some measurable physical property of the device, such as its resistance, which can then be measured electronically. These detectors are generally insensitive to the wavelength of the incident radiation, but usually have large areas to increase their sensitivity. These factors make them relatively unimportant in the field of optoelectronic sensors, although they do form the basis of most laser power meters. Typical examples are:

1.1 Thermoelectric detectors

These rely on the principle of the thermocouple (the Seebeck effect) whereby the heating of one junction between two dissimilar metals relative to the other causes a current to flow round a circuit that is proportional to the temperature difference between the junctions. Their usefulness lies in their simplicity and their rugged construction.

1.2 The Bolometer

Here the incident radiation heats a fine wire or metallic strip causing a change in its electrical resistance, which is then measured in a variety of ways. The performance of these devices depends upon the temperature coefficient of resistance of the material. Thermistors are similar, but rely on semiconducting elements such as oxides of manganese, cobalt or nickel. Carbon resistance bolometers cooled to liquid helium temperature (4.2 K) have proved successful in far-IR astronomy where very sensitive detectors are required.

1.3 Pneumatic Detectors

The receiving element in a pneumatic detector is placed in an airtight chamber. Radiation falling on the element causes the air temperature inside the chamber to rise and hence the air pressure to increase. This pressure change is then detected in a number of ways, including the use of a flexible mirror, whose distortion moves a beam of light in a controlled and measurable fashion (known as a Golay cell detector).

1.4 Pyroelectric Detectors

The incident radiation is absorbed in a ferroelectric material which has molecules with a permanent electric dipole moment. The net electric polarisation present is temperature dependent (below the a critical temperature characteristic of the material). When configured as a capacitor in a circuit, changes in polarisation induced by temperature changes in the material can be detected by measuring the change in the charge on the plates of the capacitor. Pyroelectric detectors can be made with response times in the nanosecond region and with a wavelength response extending out to $\sim 100\ \mu\text{m}$. They have proved very useful as low cost, robust IR detectors in such uses as fire detection and intruder alarms.

2 Photon Devices - Photoemissive Detectors

When photons with a wavelength less than a critical value are absorbed by a metal, electrons are emitted (the photoelectric or photoemissive effect). The electrons must have energies greater than the surface work function ϕ , and are emitted with kinetic energies up to

$$E = h\nu - e\phi.$$

No electrons will be emitted if $h\nu < e\phi$ (or $\lambda_0 > hc/e\phi$). This is illustrated in figure 5.1. If inelastic collisions are present the only a fraction of the electrons with this energy may escape. The ratio of the number of emitted electrons to the number of absorbed photons is called the *quantum yield* or *quantum efficiency*.

Pure metals have low quantum efficiencies ($\sim 0.1\%$), and high work functions. Two types of photocathode are used in practice. The older classical types consist of thin evaporated layers of alkali metals. They are often designated by an 'S' number. They may be regarded as semiconductors where electrons must gain an energy of at least

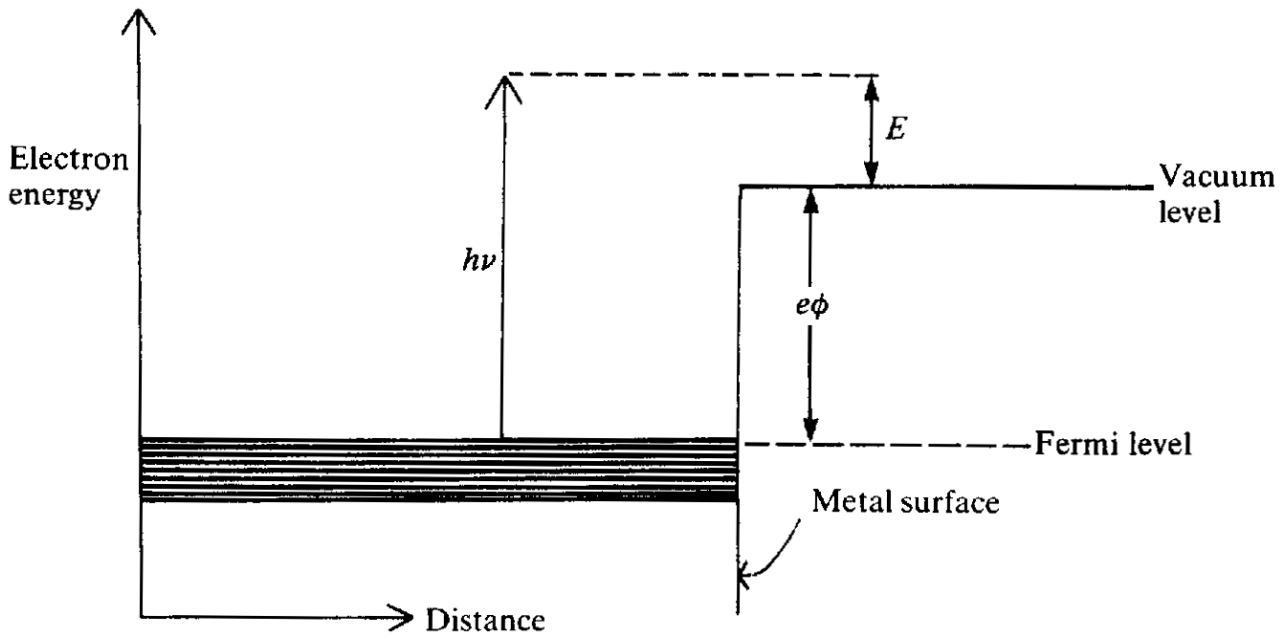


Figure 5.1 Electron energy level diagram at a metal/vacuum interface illustrating the photoelectric effect. To escape from inside the metal, an electron must gain at least an energy $e\phi$, where ϕ is the work function.

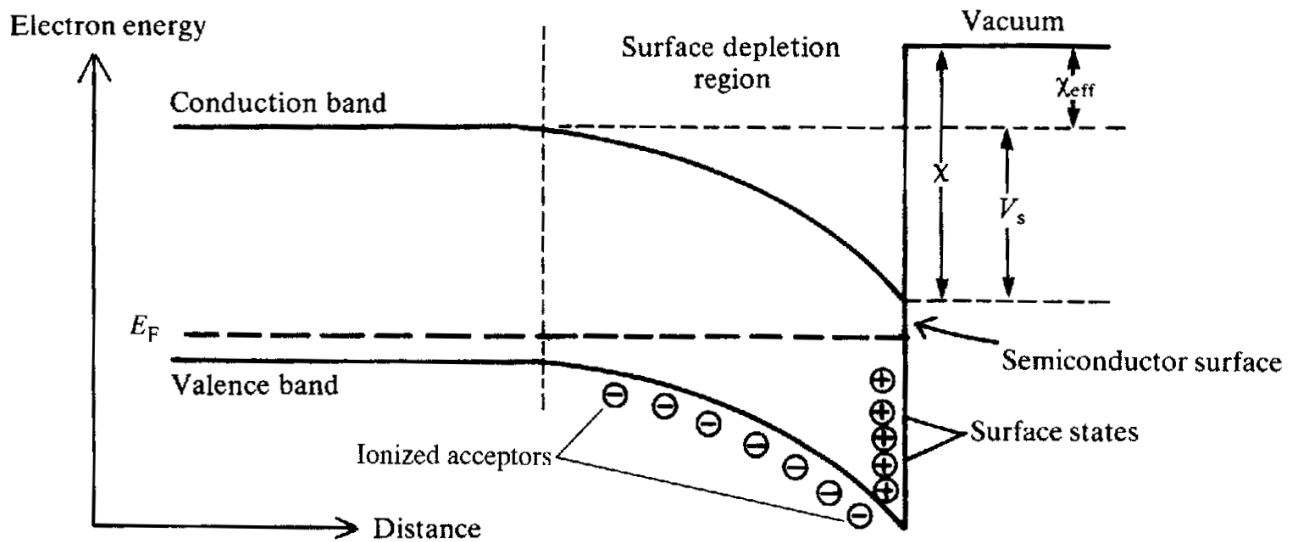


Figure 5.2 The effective electron affinity of a semiconductor may be altered if band bending takes place at the surface. Here holes trapped in surface states cause a surface depletion region to be formed. The potential drop V_s across the depletion region reduces the effective electron affinity for bulk electrons from χ to $\chi - V_s$.

$E_g + \chi$ (where E_g is the energy gap and χ is the electron affinity) to escape from the surface. The material NaKCsSb is a typical multi-alkali photocathode, known as S20, it has $E_g = 1.0$ eV and $\chi \approx 0.4$ eV, and hence it should have a threshold photon energy of ~ 1.4 eV, which is indeed close to that observed.

Newer photocathodes reduce the effective value of χ by making use of *band bending* and are known as *negative electron affinity* or (NEA) types. The band bending is illustrated in figure 5.2, and is found to occur when there are states within the energy gap at the semiconductor surface. A depletion region is formed, very similar to that found in a p-n junction. The potential drop V_s across the depletion region leads to band bending as shown. The effective electron affinity then becomes

$$\chi_{\text{eff}} = \chi - V_s.$$

If $V_s > \chi$ then we have a negative electron affinity and the effective work function for bulk electrons is just E_g . In practice, NEA photocathodes are formed by evaporating caesium oxide onto the semiconductor surface. Photocathodes using GaAs operate at quite high quantum efficiencies right up to the energy gap of GaAs at $\sim 0.9 \mu\text{m}$. The quantum efficiencies of a number of the more common photocathode materials are shown as a function of wavelength in figure 5.3.

Vacuum photodiodes are the simplest devices based on the above process. They require large optical powers to produce relatively modest outputs, and therefore a much more common and important device is the photomultiplier. In the photomultiplier the photoelectrons are accelerated towards a series of electrodes (called *dynodes*) which are maintained at successively higher potentials with respect to the cathode. On striking a dynode surface, each electron causes the emission of several secondary electrons, which in turn are accelerated towards the next dynode and continue the multiplication process. If, for example, 5 electrons are emitted at each dynode, and there are 9 dynodes, then a gain of $G = 5^9 = 1.95 \times 10^6$ is possible. Thus photomultipliers offer significant amplification. Four of the most common types of photomultiplier dynode configurations are illustrated in figure 5.4.

Photomultipliers or PMTs are highly sensitive devices, but have the disadvantage of being relatively bulky. It is possible to obtain PMTs with risetimes ~ 1 ns. If monochromatic radiation with a vacuum wavelength of λ_0 and power P_λ is incident on a photocathode then the number of photons N_p incident per second is given by

$$N_p = \frac{P_\lambda}{hc/\lambda_0} = \frac{P_\lambda \lambda_0}{hc}$$

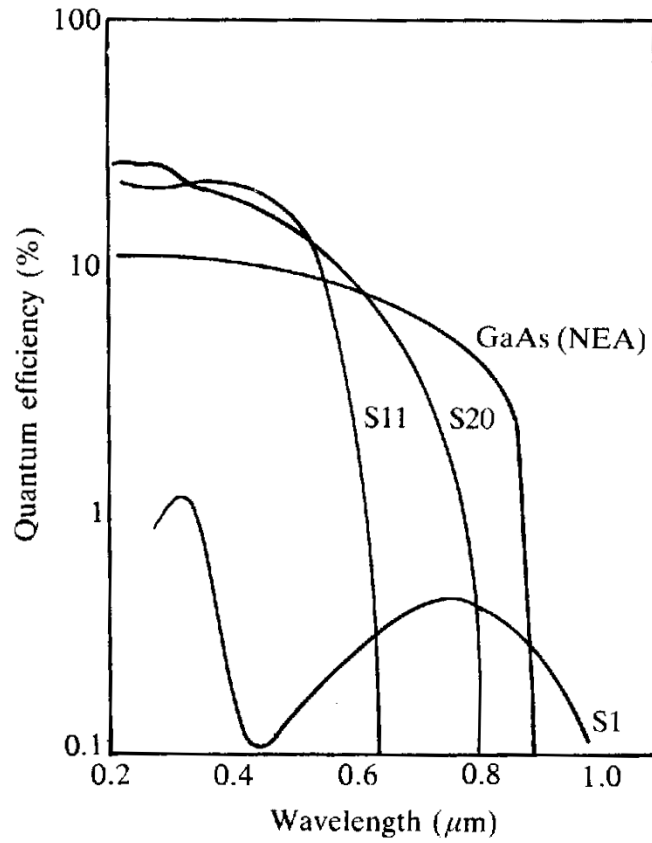


Figure 5.3 Quantum efficiency versus wavelength for a number of the more common photocathode materials.

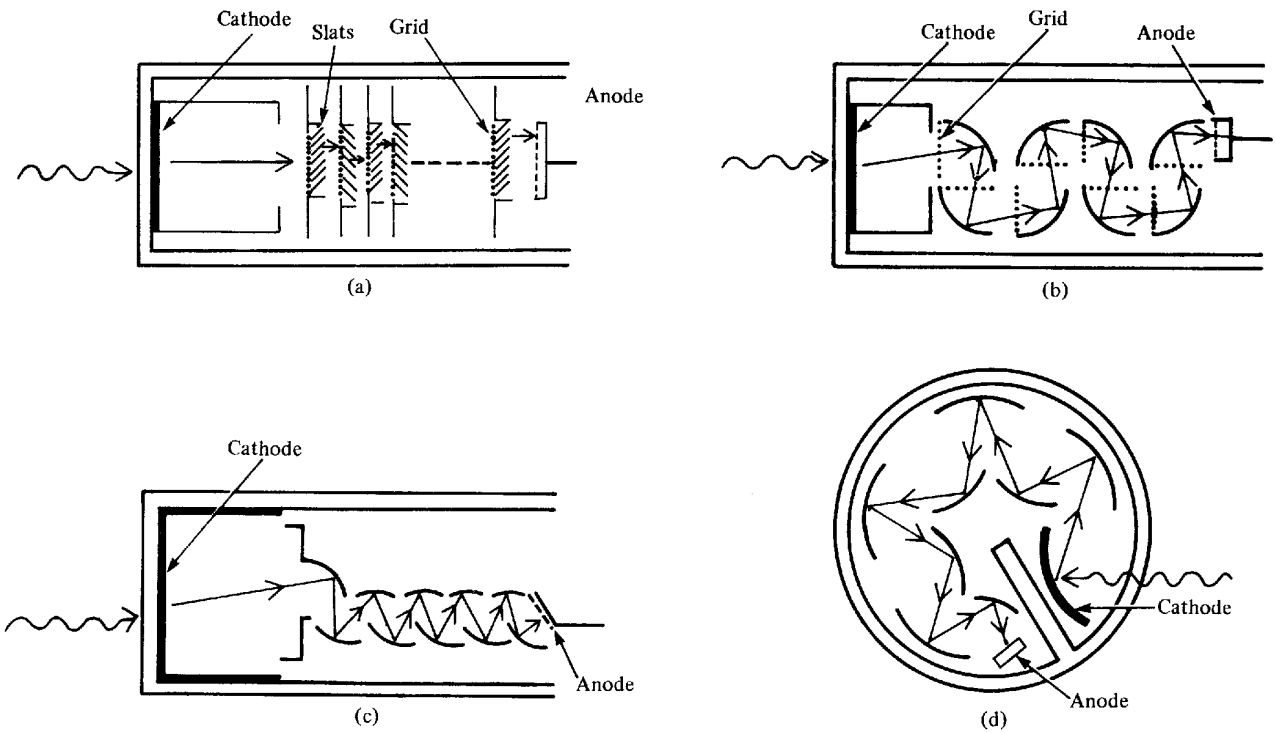


Figure 5.4 Dynode structures of four common types of photomultiplier: (a) venetian blind; (b) box and grid; (c) linear focused and (d) circular cage focused. Typical electron trajectories through the system are also shown.

and hence if the quantum efficiency of the photocathode is η then the current flowing through the external circuit, i_λ , is given by

$$i_\lambda = \frac{\eta e P_\lambda \lambda_0}{hc}$$

and the responsivity R_λ is given by

$$R_\lambda = \frac{i_\lambda}{P_\lambda} = \frac{\eta e \lambda_0}{hc}.$$

Even when no radiation is falling on the photocathode, thermionic emission gives rise to a **dark current** which often constitutes the main source of noise in PMTs. The thermionic emission current i_T for a cathode at temperature T of area A and work function ϕ is given by the Richardson–Dushman equation (see Blakemore, *Solid State Physics*)

$$i_T = aAT^2 \exp\left(-\frac{e\phi}{k_B T}\right)$$

where a is a constant, which for pure metals is $1.2 \times 10^{-6} \text{ Am}^{-2}\text{K}^{-2}$. Dark current can therefore be reduced by cooling the PMT, typically to temperatures $\sim 240 \text{ K}$. Another important source of noise in PMTs is **shot noise**. This arises from the random generation and flow of charge carriers, and is related to the discrete nature of the electronic charge. An exhaustive treatment of noise is beyond this lectures course, but Yariv's book *Optical Electronics in Modern Communications* has a complete discussion of the topic. I shall be using some of the more well-known results of noise analysis without formal proof. Thus the magnitude of the r.m.s. current fluctuations Δi_s with frequencies between f and $f + \Delta f$ is given by

$$\Delta i_s = (2ie\Delta f)^{1/2}$$

where i is the current flowing (the sum of the dark current and signal current). Therefore the minimum detectable signal power in the presence of a thermionic dark current i_T is given by

$$P_{\min} = \frac{(2i_T e \Delta f)^{1/2}}{R_\lambda}.$$

Thus it is now possible to make an estimate of the minimum signal power. For a cathode of area 1000 mm^2 , a work function ϕ of 1.25 eV and a cathode temperature of 300 K (giving $k_B T/e = 0.025 \text{ eV}$) we have for i_T

$$i_T = 1.2 \times 10^6 \times 10^{-3} \times (300)^2 \exp(-1.25/0.025) = 2 \times 10^{-14} \text{ A}$$

At a wavelength of 500 nm and a quantum efficiency η of 0.25 the responsivity is

$$R_\lambda = \frac{\eta e \lambda_0}{hc} = \frac{0.25 \times 1.6 \times 10^{-19} \times 0.5 \times 10^{-6}}{6.6 \times 10^{-34} \times 3 \times 10^8} = 0.1 \text{ AW}^{-1}$$

Finally, if we take a bandwidth of 1 Hz then the minimum detectable signal power is

$$P_{\min} = \frac{(2 \times 2 \times 10^{-14} \times 1.6 \times 10^{-19} \times 1)^{1/2}}{0.1} = 8 \times 10^{-16} \text{ W}$$

This is equivalent to around 2000 photons. Thus if the photocathode is cooled, individual photons can be detected by these devices.

Two other important noise sources for PMT tubes are **multiplication noise**, which comes from the dynode chain, but is usually a small contribution to the total noise (20%) and **Johnson** or **Nyquist noise**. Johnson noise arises because of the thermal agitation of the charge carriers within a conductor; the random nature of this motion results in a fluctuating voltage appearing across the conductor. The r.m.s. value of this voltage ΔV_J having frequency components between f and $f + \Delta f$ across a resistance R at a temperature T is given by

$$\Delta V_J = (4k_B T R \Delta f)^{1/2}$$

In a PMT such noise will appear across a load resistor at the anode. In practice, Johnson noise is also much smaller than the dark-current shot noise.

Image intensifiers are another important class of devices based on the PMT principle. They are intended to boost very low intensity optical images to the point where they become useful. They can also act as wavelength down-converters in that they can convert near-IR radiation into visible radiation. There are many different designs in use, but one of the most popular recently is called the **microchannel plate image intensifier** or MCP. The device is illustrated in figure 5.5. The MCP consists of a slab of insulator ($\sim 500 \mu\text{m}$ thick) with a high density of smaller diameter ($\sim 15 \mu\text{m}$) holes or *channels* in it. The inner faces of the channel are made slightly conducting and a potential ($\sim 1 \text{ kV}$) is applied between opposite faces of the slab as shown. Electrons entering one of the channels are accelerated down it and strike the walls soon after entering. As in the PMT, secondary electrons are generated by the impact and the process is repeated down the channel as illustrated. The electron shower then strikes the phosphor and a pixellated image is produced.

3 Photon Devices - Photoconductive Detectors

In these semiconductor based detectors light whose energy is greater than that of the bandgap causes the generation of electron-hole pairs. As long as the electron remains in

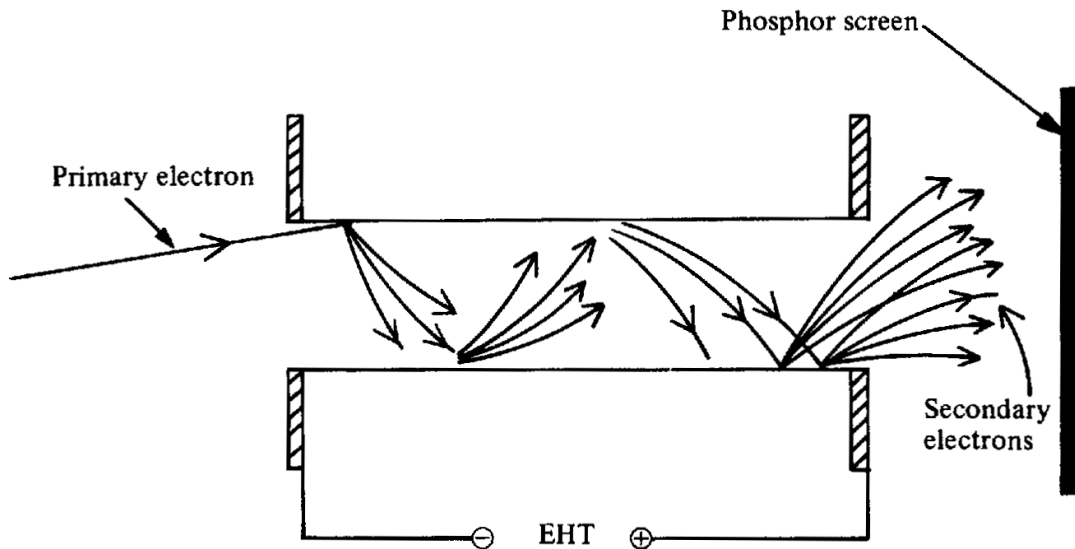


Figure 5.5 Electron multiplication in a microchannel plate image intensifier. When the primary electrons enter the channel and strike the walls, secondary electrons are emitted that in turn generate further secondaries. The channel thus acts as a miniature photomultiplier tube. On emerging from the channel the electrons generate light by striking a phosphor screen.

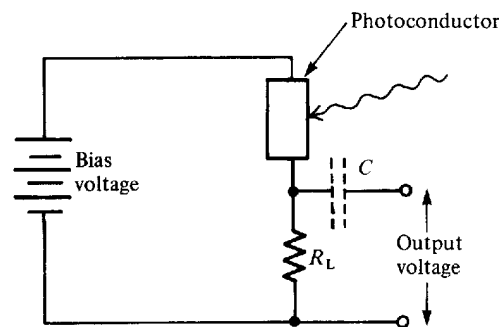
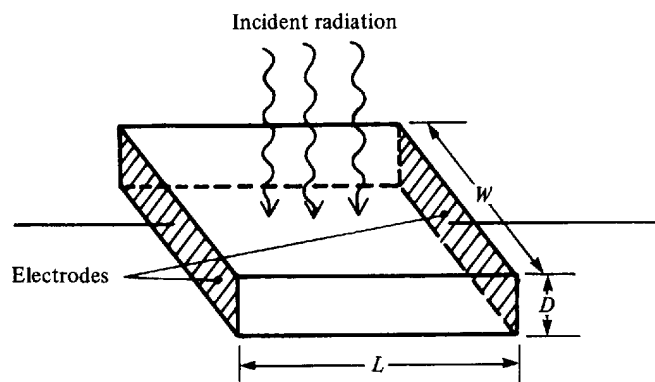


Figure 5.6 (a) Geometry of a slab of photoconductive material. The slab of length L , width W and thickness D has electrodes on opposite faces; radiation falls onto the upper face. (b) Photoconductor bias circuit. Changes in the resistance of the photoconductor cause changes in the voltage appearing across R_L .

the conduction band, the conductivity of the semiconductor will be increased. This is the phenomenon of photoconductivity, which is the basic mechanism operative in photoconductive detectors. A typical detector geometry and circuit is shown in figure 5.6. Any change in the conductivity of the detector results in an increased flow of current around the circuit, which will increase the potential across the load resistor R_L . Figure 5.7 shows the variation of the optical absorption coefficient α for several semiconductors. The irradiance $I(x)$ at a point a distance x into a semiconductor can thus be written as

$$I(x) = I(0) \exp(-\alpha x)$$

This means that the fraction of the incident irradiance which is actually absorbed in the semiconductor is

$$\eta = (1 - R) \times [1 - \exp(-\alpha D)]$$

where R is the intensity reflection coefficient and D is the thickness of the slab. The wavelength response of photoconductive detectors should, in theory increase linearly up to λ_g , although the variation of α with wavelength means that η often decreases faster at short wavelengths.

In the visible region of the spectrum these devices are often used as light meters in cameras (using CdS and CdSe detectors). They usually have high gains but poor response times (~ 50 ms). In the near IR lead sulphide (PbS) is often used as a detector material, with a useful wavelength response from $1 \mu\text{m}$ to $3.4 \mu\text{m}$. Typical response times are $\sim 200 \mu\text{s}$. Another important photoconductive detector in the far-IR is mercury cadmium telluride ($\text{Hg}_x\text{Cd}_{1-x}\text{Te}$). This compound may be thought of as an alloy composed of the semimetal HgTe and the semiconductor CdTe. Consequently, depending upon the composition of the alloy, a semiconductor may be formed with a bandgap varying between zero and 1.6 eV. Real detectors have peak sensitivities in the range $5 - 14 \mu\text{m}$, and need to be cooled. The detectors are useful as they can detect black body radiation from live tissue. Early television cameras used devices called vidicons, which are electron tubes where photoconductive elements form the target, which is then read by a scanning electron gun. These have now largely been superseded by CCD detectors, as will be discussed later.

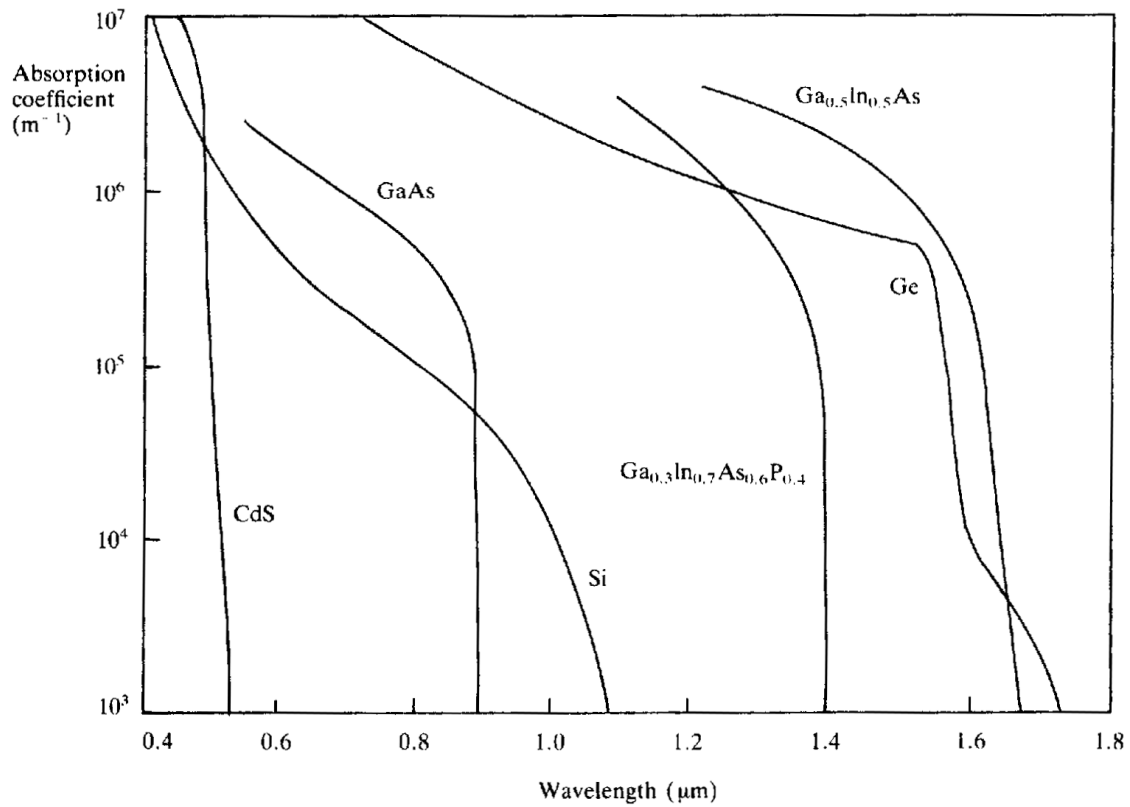


Figure 5.7 Variation of the optical absorption coefficient α with wavelength for several semiconductor materials.

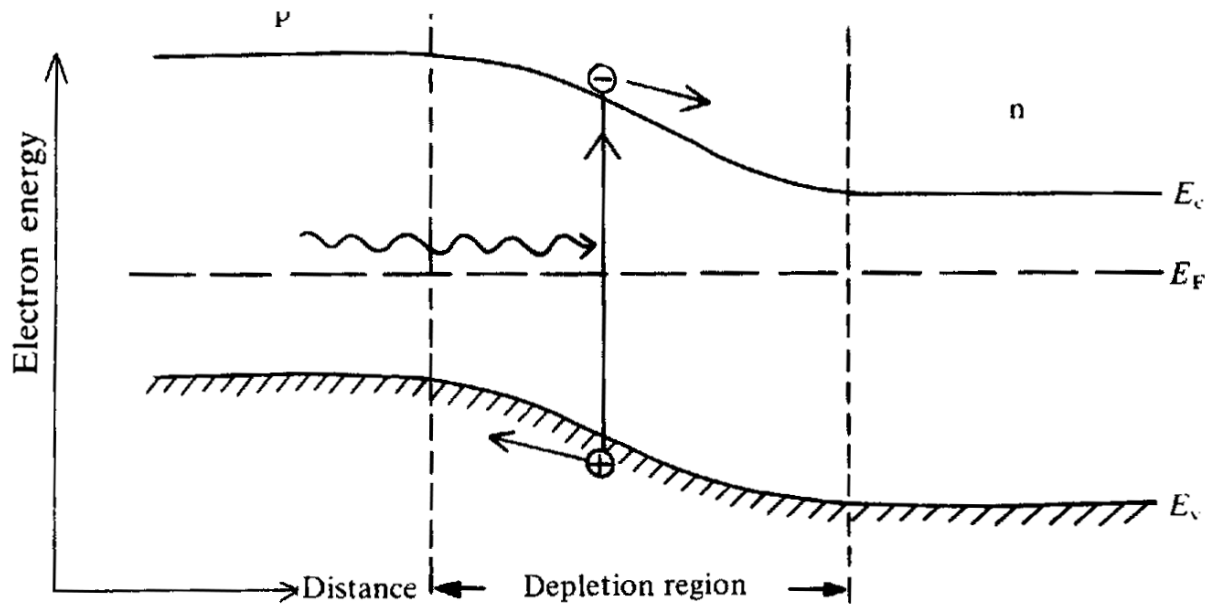


Figure 5.8 Electron energy diagram showing the generation and subsequent separation of an electron-hole pair by photon absorption within the depletion region of a p-n junction.

4 Photon Devices - Junction Detectors

All junction detectors, as the name implies, are based in some way on the humble p–n junction. When a p–n junction is formed in a semiconductor material, a region depleted of mobile charge carriers is created that has a high internal electric field across it. If an electron–hole pair is generated by photon absorption within this region the electric field separates the charges as illustrated in figure 5.8.

The charge separation may be detected in three distinct ways. First, if the device is left on open circuit an externally measurable potential will appear between the p and n regions; this is the *photovoltaic* mode of operation. Secondly, in the *photoamperic* mode a very low external resistance is connected between the external contacts and a photogenerated current flows through it. Finally, the most usual way to operate the device is in the *photoconductive* mode where a reverse bias is applied across the junction and the resulting current flow through an external load resistor measured. The load resistor in this case need not be as small as in the photoamperic mode. The photoconductive mode is preferred in practical detectors because the external current flowing in the detector circuit is directly proportional to the incident light irradiance over a relatively wide dynamic range. It also offers a more rapid response than other modes. One disadvantage is the presence of a dark current which, as in the PMT, gives rise to shot noise and limits the ultimate sensitivity of the device. The responsivity in this mode can be written as

$$R_\lambda = \frac{\eta e \lambda}{hc} = \frac{\eta \lambda}{1.24} \text{ AW}^{-1}$$

If we use a typical value for η of 0.8 and a wavelength of $0.85 \mu\text{m}$ in silicon, we get a value for R_λ near to the peak of $R_\lambda \sim 0.55 \text{ AW}^{-1}$.

A typical structure for a p–n junction diode is shown in figure 5.9. The resulting electric field variation within the depletion regions is shown in figure 5.10. For efficient detection the electron–hole pairs should be generated within the depletion region. At short wavelengths, where the absorption coefficient is relatively high, they will be generated close to the surface. Consequently, to achieve a good short wavelength response, the p^+ region should be made as thin as possible. Conversely, at the upper wavelength range of the detector the absorption coefficient will be relatively small and a wide depletion region is required for high detection efficiency. This is controlled by the reverse bias voltage, which is limited by the diode breakdown voltage. Detection efficiency may also be improved by providing an anti-reflection coating to the front surface of the detector, consisting of a $\lambda/4$ thick layer of SiO_2 .

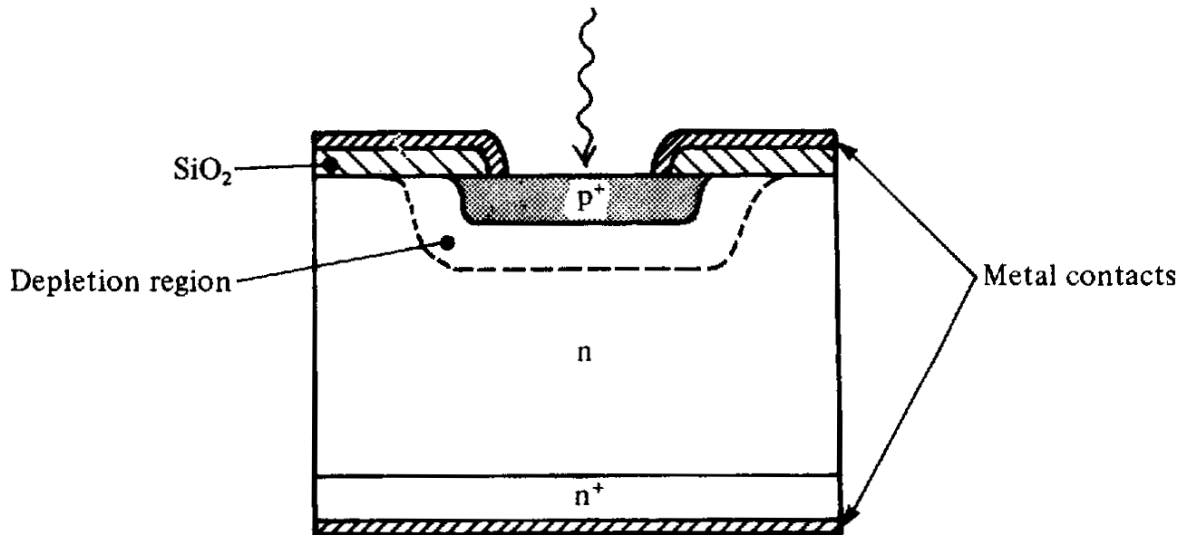


Figure 5.9 Typical silicon photodiode structure for photoconductive operation. A junction is formed between heavily doped p-type material (p^+) and fairly lightly doped n-type material so that the depletion region extends well into the n-type material. The p^+ layer is made fairly thin. Metallic contacts can be made directly to the p^+ material, but to obtain an ohmic contact to the n-type material an intermediate n^+ layer must be formed.

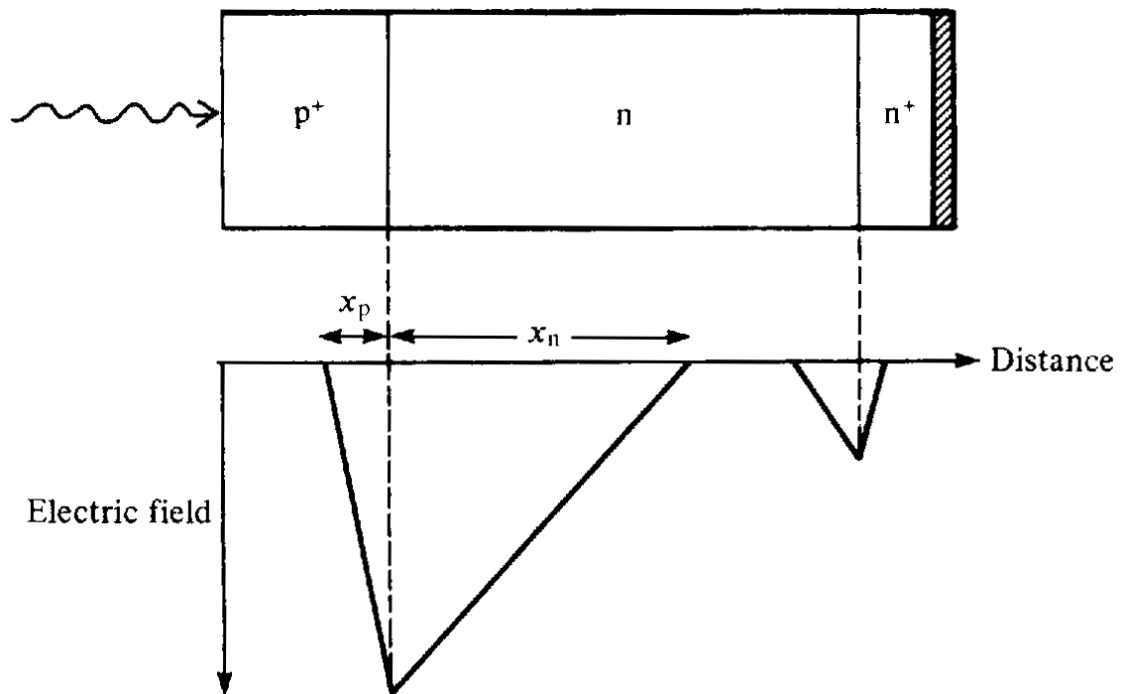


Figure 5.10 Electric field distribution within the p^+ - n junction diode shown above, assuming an abrupt diode structure.

The bandwidth of the photodiode is related to the circuit used. There are three factors which contribute to the circuit's response time: (a) the time taken by the photo-generated carriers to drift across the depletion layer, (b) the time taken by the carriers to diffuse through the respective p or n materials to the contacts and (c) the RC time of the electrical circuit.

For (a), the time depends upon both the drift velocity of the carriers and the width of the layer. In Si the maximum velocity for the carriers is $\sim 5 \times 10^4 \text{ ms}^{-1}$ and a typical depletion width is $\sim 2.5 \mu\text{m}$, thus the response time becomes $\sim 50 \text{ ps}$ and the bandwidth is $\sim 20 \text{ GHz}$. For (b) the diffusion time must also be minimised. Since diffusion velocities are generally lower than drift velocities the p and n regions must be made quite narrow. Thicknesses of $0.5 \mu\text{m}$ are normally used. Finally, for (c), a typical p-n junction capacitance is $\sim 25 \text{ pF}$, so for a 20 GHz bandwidth, we require

$$R < \frac{1}{2\pi fC} = 0.32 \Omega.$$

This is a small value for the resistance, necessitating the use of a carefully constructed amplifier. If the more usual 50Ω value is chosen, then the bandwidth becomes $\sim 100 \text{ MHz}$. This is more than sufficient for the vast majority of applications (but these do not include high-bit-rate optical communications!).

4.1 Noise in p-n junctions

What of noise in p-n junctions? The shot noise is given by the expression quoted earlier for the PMT as

$$i_n = (2i_D e \Delta f)^{1/2}$$

where i_D is the current flowing through the circuit. This will be the sum of two components

$$i_D = i_P + i_d$$

where i_P is the photogenerated current and i_d is the dark current, which is due to leakage of thermally generated charge carriers across the junction. It depends both on the temperature of the device and on its area. The noise performance of the diode itself is usually expressed in the form of the **noise equivalent power** (NEP), which is the optical power input which would produce a photocurrent equal to the dark current, i_d . Again, by analogy with the PMT we have

$$\text{NEP} = \frac{h\nu(2ei_d\Delta f)^{1/2}}{e\eta}.$$

It is quoted as a power ‘per root hertz’, in other words, for unit bandwidth. A typical value for the NEP for a Si photodiode is $\sim 10^{-14} \text{ WHz}^{-1}$, corresponding to dark currents of $\sim 1 \text{ nA}$.

To get the whole noise picture the load resistor and the rest of the circuit discussed above needs to be included. Thus the Johnson noise current in the resistor will be

$$i_R = \left(\frac{4k_B T \Delta f}{R} \right)^{1/2}$$

and hence the total circuit noise will be

$$i_N = (2i_d e \Delta f)^{1/2} + \left(\frac{4k_B T \Delta f}{R} \right)^{1/2}$$

The relative values of these two terms depend upon the relative values of i_d and R . As R is typically 50Ω for fast circuits, and $i_d \sim 1 \text{ nA}$, thermal noise normally dominates.

4.2 p-i-n diodes

As a detector the p-i-n photodiode has a number of advantages over the p-n photodiode. A p-i-n diode is a p-n junction with an intrinsic (usually lightly doped) layer sandwiched between the p and n layers. It may be operated under a variety of bias conditions. The energy band diagram, charge distribution and electric field distribution for a reverse-biased p-i-n diode are illustrated in figure 5.11. This structure serves to extend the width of the region supporting an electric field, in effect widening the depletion layer. Photodiodes with p-i-n structure offer the following advantages:

- (a) Increasing the width of the depletion layer of the device (where the generated carriers can be transported by drift) increases the area available for capturing photons.
- (b) Increasing the width of the depletion layer reduces the junction capacitance and thereby the RC time constant. On the other hand, the transit time increases with the width of the depletion layer.
- (c) Reducing the ratio between the diffusion length and the drift length of the device results in a greater proportion of the generated current being carried by the faster drift process.

Response times in tens of ps, corresponding to bandwidths of $\sim 50 \text{ GHz}$, are achievable. The responsivity of two commercially available p-i-n photodiodes is compared with that of an ideal device in figure 5.12. It is interesting to note that the responsivity maximum occurs for wavelengths substantially shorter than the bandgap wavelength. This is because Si is an indirect gap material.

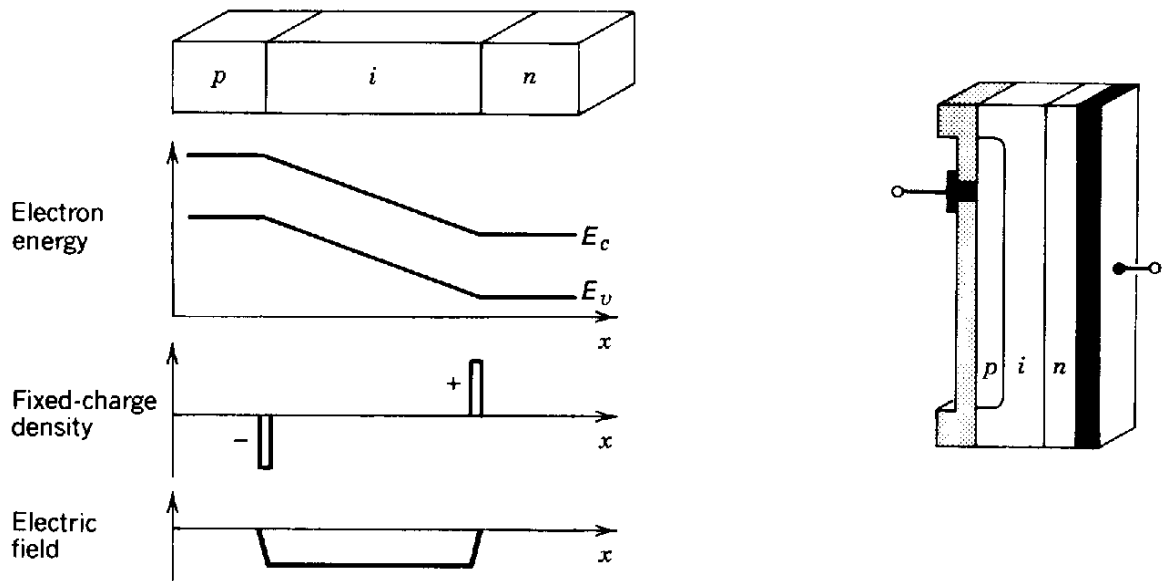


Figure 5.11 The p-i-n photodiode structure, energy diagram, charge distribution and electric field distribution. The device can be illuminated either perpendicularly or parallel to the junction.

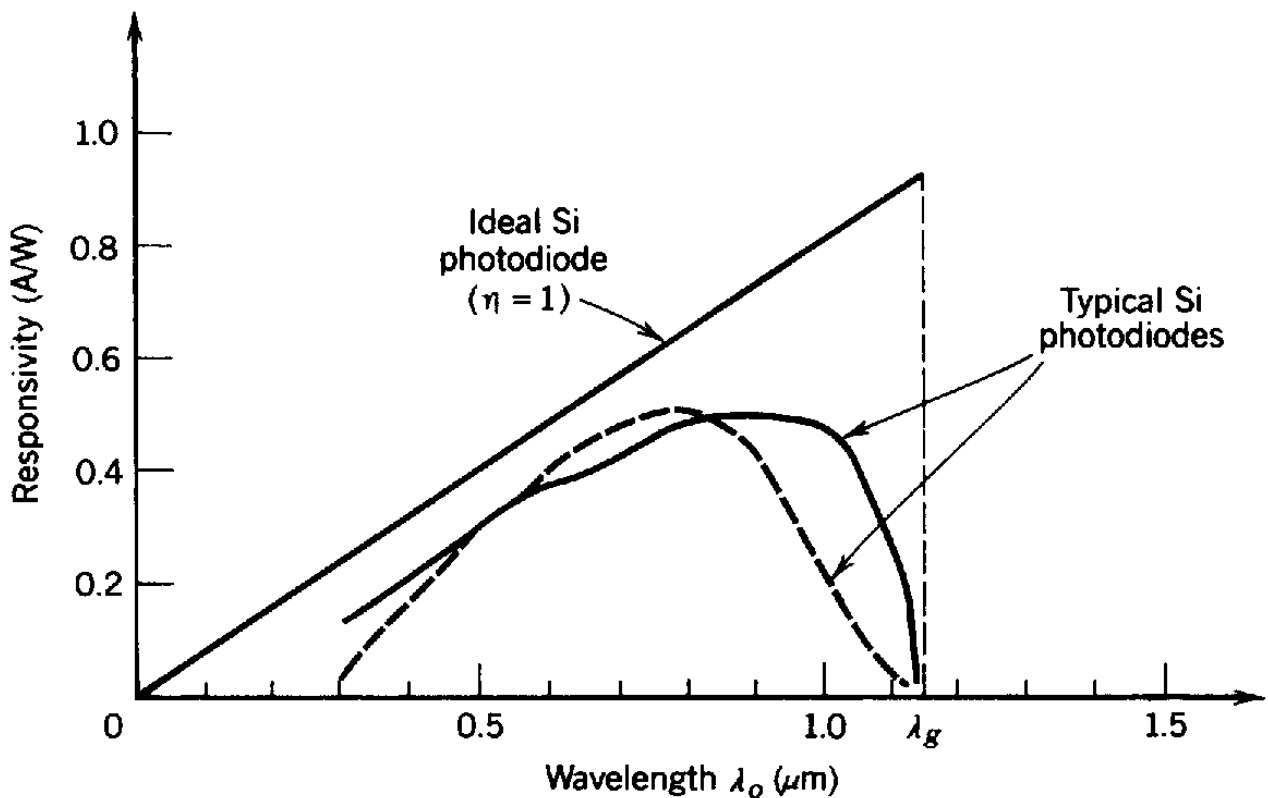


Figure 5.12 Responsivity versus wavelength for ideal and commercially available Si p-i-n photodiodes.

In fibre-optic communication systems, the wavelengths of interest are $1.3\ \mu\text{m}$ and $1.5\ \mu\text{m}$. Thus there is a demand for photodiodes which have high sensitivities and exceptionally wide bandwidths. These are generally made from heterojunctions of semiconductor alloys, generally grown on InP substrates. These include the ternary compound $\text{In}_x\text{Ga}_{1-x}\text{As}$ and the quaternary compound $\text{In}_x\text{Ga}_{1-x}\text{As}_y\text{P}_{1-y}$. A typical structure is shown in figure 5.13, where an i layer of $\text{In}_{0.53}\text{Ga}_{0.47}\text{As}$ is sandwiched between a p^+ layer of InP and an n layer of InP. Because the radiation has to pass through a layer of InP which has a bandgap wavelength of $0.92\ \mu\text{m}$, then no radiation below this wavelength will be detected. A further advantage of this structure is that since no carriers of interest will be generated in either the surface p^+ layer or the lower n layer there will be no diffusion carriers to the junction from outside the depletion region, thus improving the response time. From figure 5.7 it can be seen that the absorption coefficient of $\text{In}_{0.53}\text{Ga}_{0.47}\text{As}$ is much higher near the bandedge than that of Si. This is because $\text{In}_{0.53}\text{Ga}_{0.47}\text{As}$ is a direct gap material. This means that thinner active layers ($\sim 2\ \mu\text{m}$) can be used, again improving the response speed. Typical values are $\sim 30\ \text{ps}$.

4.3 Avalanche photodiodes

An **avalanche photodiode** (APD) operates by converting each detected photon into a cascade of moving carrier pairs. Weak light can then produce a current that is sufficient to be readily detected by the electronics following the APD. The device is a strongly reverse-biased photodiode in which the junction electric field is large; the charge carriers therefore accelerate, acquiring enough energy to excite new carriers by the process of **impact ionization**. The process is illustrated in figure 5.14. A photon is absorbed at point 1, creating an electron-hole pair. The electron accelerates under the strong electric field, thereby increasing its energy with respect to the bottom of the conduction band. Should the electron, whilst being scattered by phonons, acquire an energy larger than E_g at any time, it has the opportunity to generate a second electron-hole pair by impact ionization (point 2). The two electrons then accelerate, and may be the source for further impact ionization. Holes also have a chance of impact ionizing, as shown at point 3. Further details of this device are available in *Physics of Semiconductor Devices* by Sze.

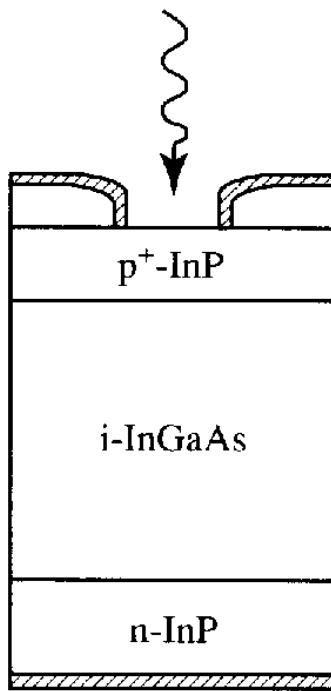


Figure 5.13 Basic structure of a p-i-n heterojunction InGaAs detector.

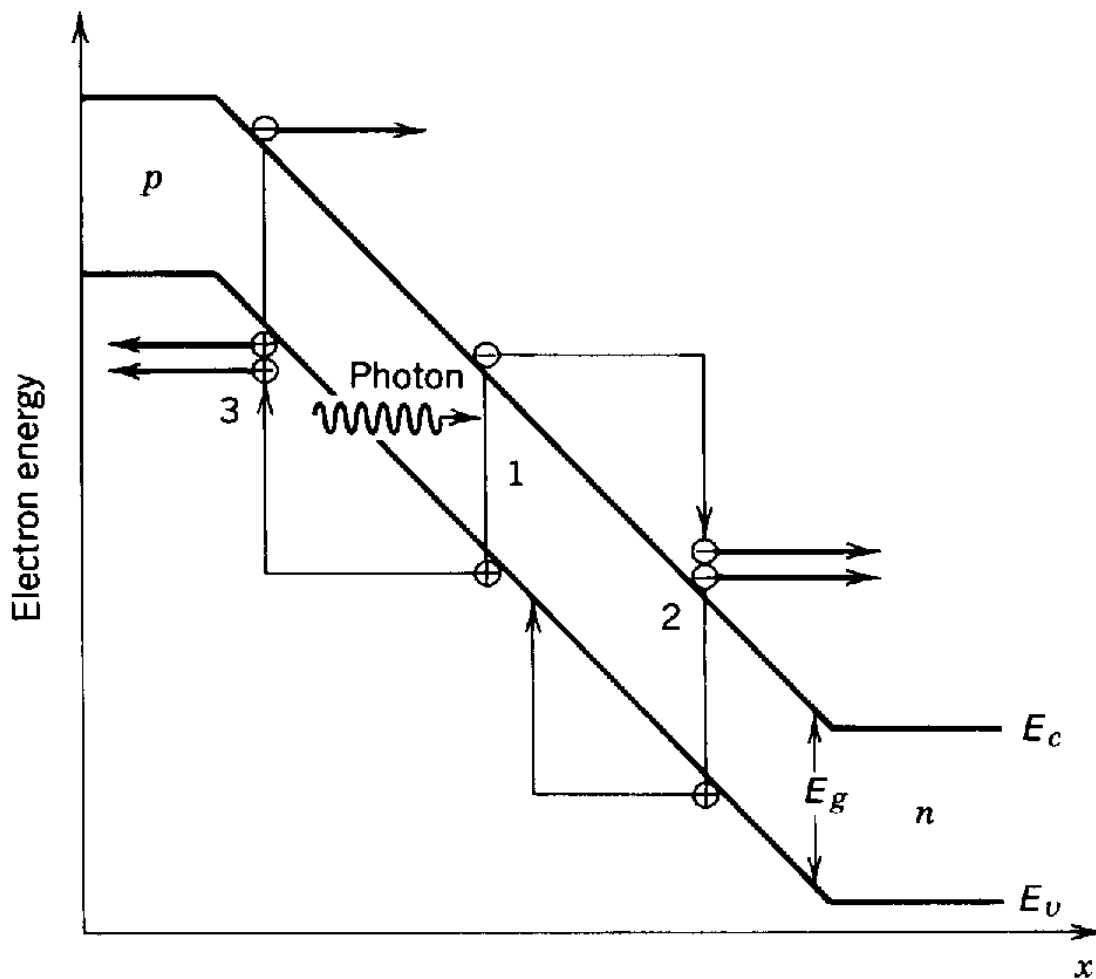


Figure 5.14 Schematic representation of the multiplication process in an APD.

5 CCD detector arrays

In the 1970s the **charge coupled device** or CCD was invented at Bell Laboratories in the U.S.A. The basic building block of this is the *metal-oxide-semiconductor* (MOS) capacitor. This is formed by growing a layer of silicon dioxide (SiO_2) on a p-type silicon substrate; a metal electrode is then evaporated on top of the oxide layer (shown schematically in figure 5.15). The metal electrode is known as the *gate* and is biased positively with respect to the silicon. Photogenerated electron-hole pairs within the silicon will be separated, with the electrons being attracted to the surface of the Si under the gate, where they will remain whilst the gate voltage is positive. The electrons are effectively trapped within a potential well formed under the gate contact. The amount of trapped charge will be proportional to the total integrated light flux falling onto the device during the measurement period.

The problem then becomes how to ‘read out’ this charge sequentially along a line of such detectors? This can be done by passing the charge from detector to detector. There are several ways of achieving this in practice. I shall illustrate the basic idea by considering a CCD where the gate potentials are supplied from three voltage lines (L_1, L_2, L_3) each one being connected to every third electrode (G_1, G_2, G_3), as illustrated in figure 5.16. Suppose that initially the potential of L_1 is at some positive value V_g , whilst L_2 and L_3 are at zero potential. Photogenerated charge will be trapped under the G_1 electrodes in proportion to the amount of light falling on these elements (figure 5.16 (b)). After a suitable integration time, the charge may be moved along the chain of MOS capacitors by applying a repeated sequence of potentials to the gate supply lines. Thus, suppose a voltage V_g is applied to L_2 whilst maintaining L_1 at V_g ; the charge initially under L_1 will now be shared between G_1 and G_2 (Figure 5.16 (c)). The potential of L_1 is then reduced to zero, and so all the charge that was initially under G_1 is now under G_2 (Figure 5.16 (d)). Thus it is possible to progressively move the charge along the line of MOS capacitors from left to right. At the end of the line, the amount of charge arriving as a function of time then provides a sequential scan of the G_1 detector outputs.

Two-dimensional arrays based on the above one-dimensional design are possible, known as *frame transfer* devices. Here the transfer registers feed into a *readout register* running down the edge of the device. The contents of each line are read out in sequence into the readout register so that the signal appearing at the end of the register represents a line-by-line scan of the image. One problem with the above scheme is that a new light

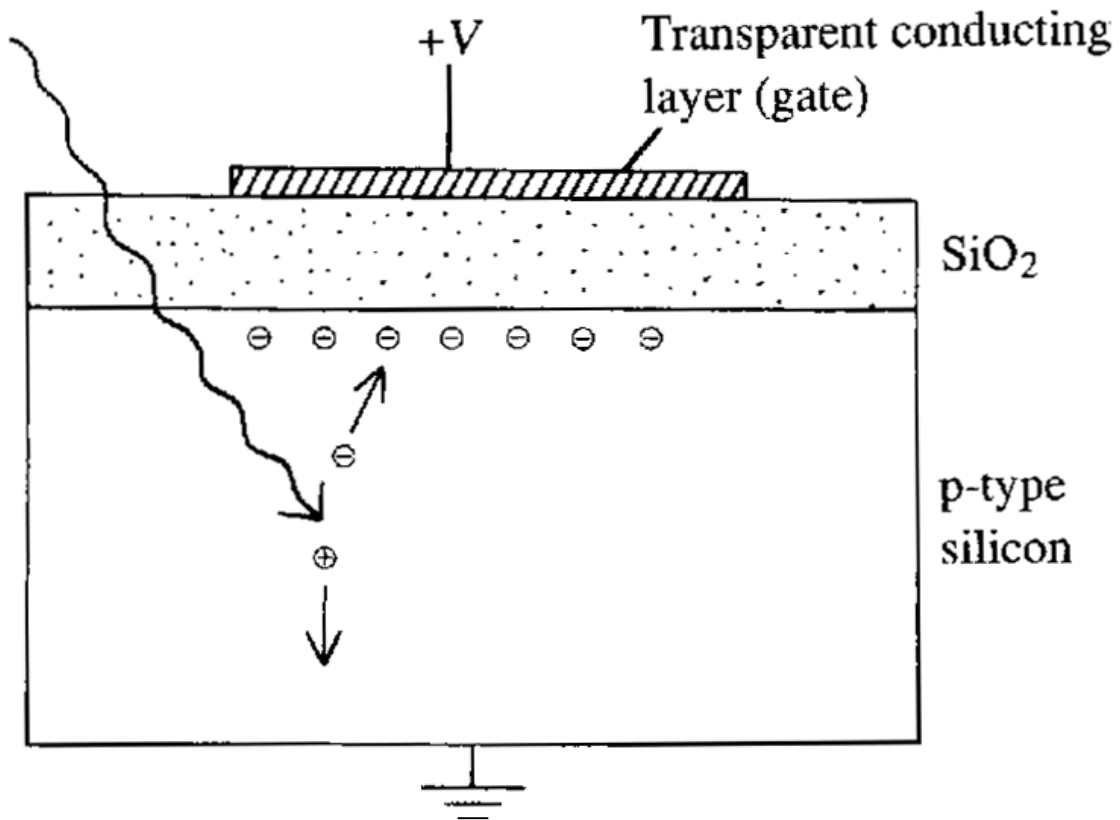


Figure 5.15 MOS capacitor structure. When the gate is biased positively, photogenerated electron-hole pairs become separated and the electrons then become trapped at the SiO₂ - Si boundary beneath the gate electrode.

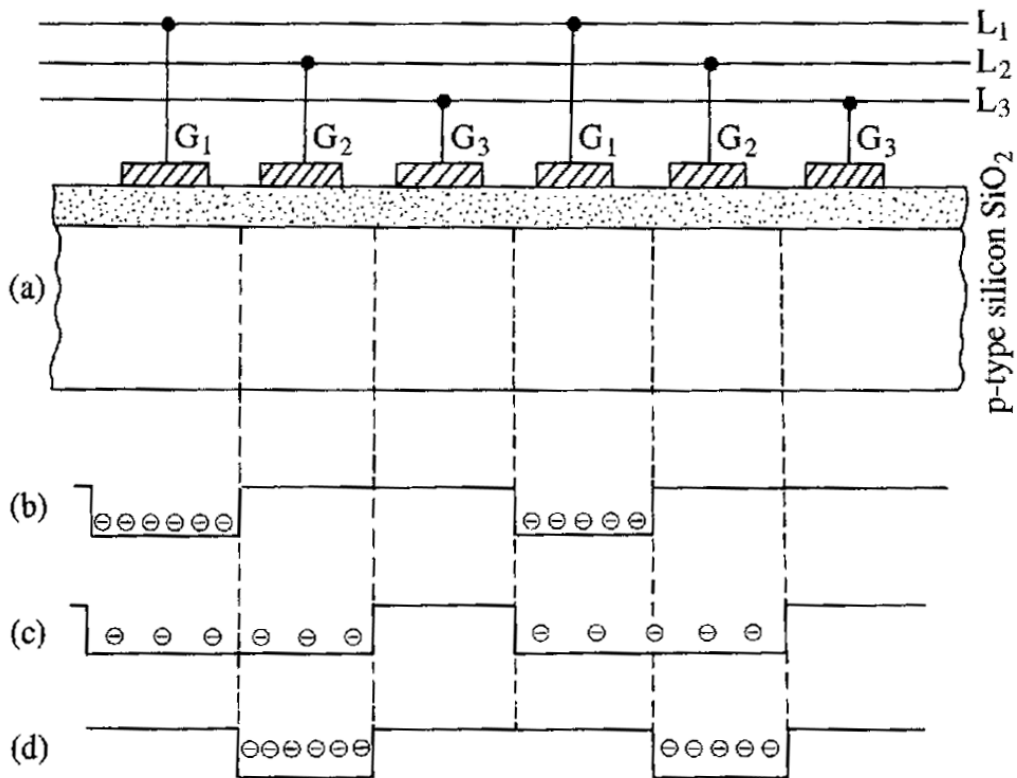


Figure 5.16 (a) Basic CCD array composed of a line of MOS capacitors. (b) The initial charge distribution within the potential wells when G_1 has a positive voltage applied (V_g) and $G_2 = G_3 = 0$. (c) $G_1 = G_2 = V_g$, $G_3 = 0$ and the charge has now spread out under both G_1 and G_2 . (d) $G_1 = 0$, $G_2 = V_g$ and $G_3 = 0$. The charge that was initially under G_1 has now moved to the right to be under G_2 . Note that no charge should be generated under the gates G_2 and G_3 ; these elements are therefore screened from incident light.

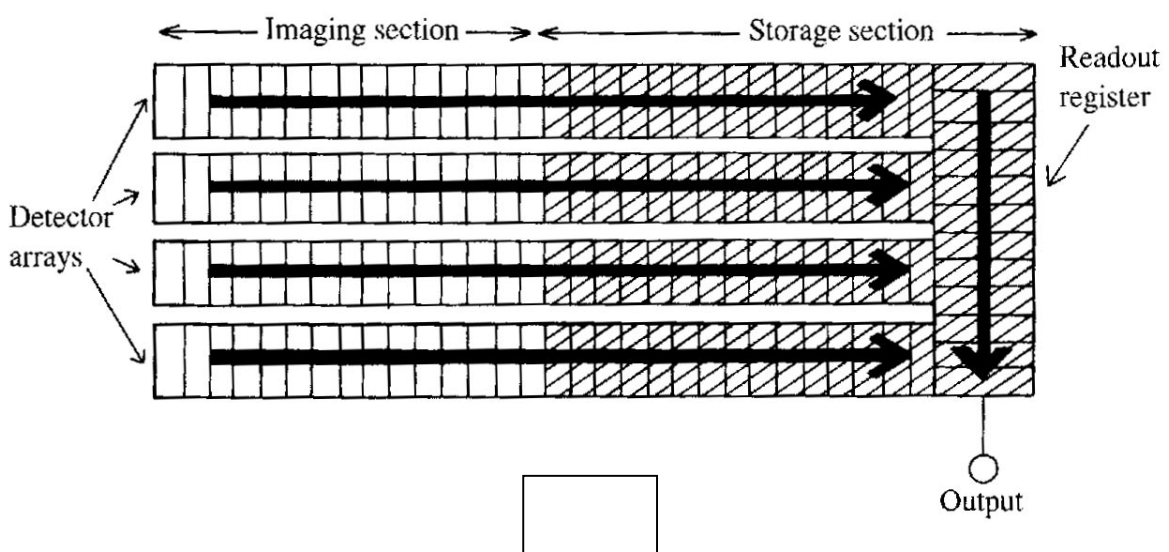


Figure 5.17 Interline transfer scheme for reading out photogenerated charge from a two-dimensional CCD image sensor. Charge flow is indicated by arrows and areas shielded from radiation by shading.

scan cannot be carried out until all of the charge has been transferred along the array. A faster scanning rate may be achieved by making each array twice as long as before, with the second half of the array being shielded from the incident radiation. Then, after a charge image has been built up it is moved along each array into the shielded section where it can be stored until it can be transferred into the readout register. Readout thus takes place whilst a new image is being built up. This is illustrated in figure 5.17.

Figure 5.18 shows a picture of a typical array. Pixel sizes can vary between $\sim 10 \mu\text{m}$ and $50 \mu\text{m}$, and arrays with over 1000 pixels are common. In modern CCDs almost no charge is lost in the transfer along the registers. Thermal excitations are a source of noise, however, and can limit the sensitivity of the device. In practice a CCD made with transparent polysilicon electrodes is now the preferred design. This can limit the quantum efficiency and so can be illuminated from below by employing a thinned substrate. The quantum efficiency can then be up to 0.9, and if cooled to 200 K the device can have almost no thermal noise. The only remaining source of noise then becomes that due to the readout electronics and A/D converter. This can be as low as one electron per pixel. Thus CCDs used for long integration exposures are the most sensitive detectors available today and routinely find application in astronomy, Raman and luminescence spectroscopy, and low light-level surveillance. At higher frame transfer rates (~ 30 frames per second) they are used in commercial TV and video cameras, as well as in still digital cameras.

When colour images are required, digital cameras use a masking technique, where red, green and blue filters are placed over successive pixels. This means that the effective resolution of the CCD is reduced by a factor of 9. As colour changes in images are usually gradual, the camera electronics then interpolate the colour information from adjacent pixels to reconstruct an image with the full pixel resolution of the CCD. This is illustrated in figure 5.19.

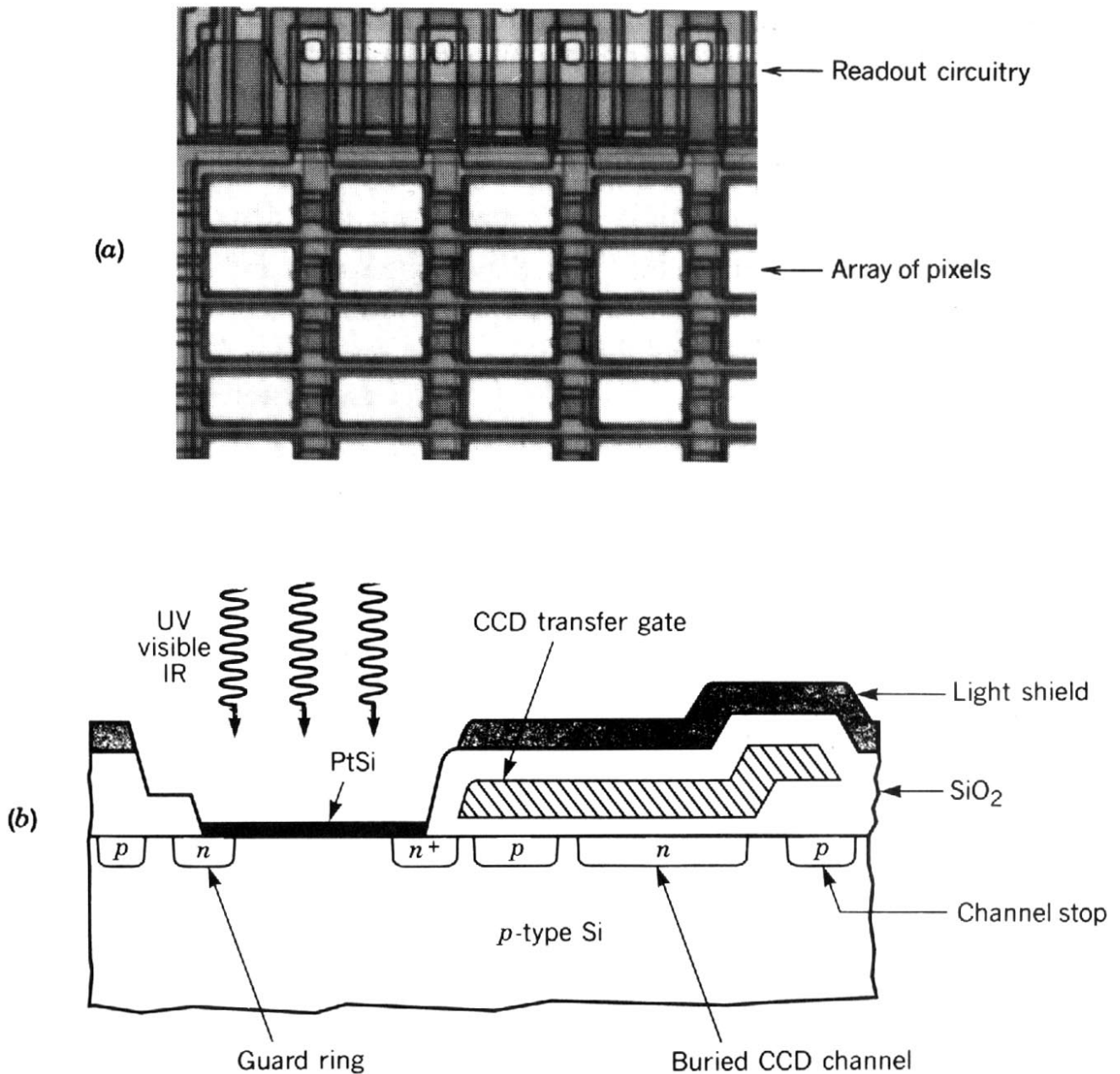


Figure 5.18 (a) Corner of an array of Schottky-barrier photodiodes. Each pixel is $40\mu\text{m} \times 80\mu\text{m}$ in size. (b) Cross-section of a single pixel in the CCD array. The light shield prevents the generation of photocarriers in the CCD transfer gate and buried channel. The guard ring minimises dark current spikes and the channel stop confines the signal charge in the lateral direction.

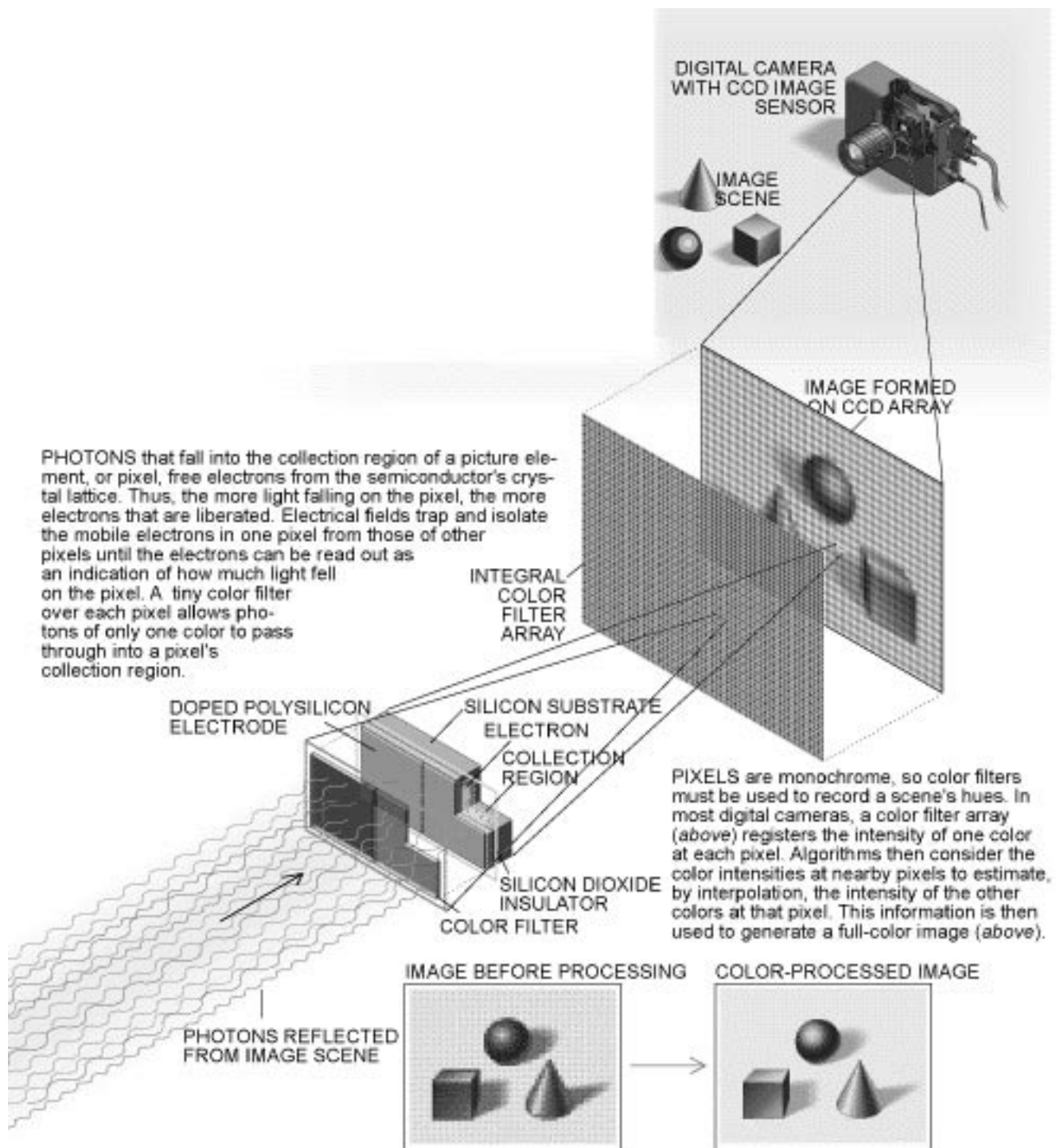


Figure 5.19 Schematic of colour CCD used in commercial digital cameras.